Age-dependent effects in the transmission and control of COVID-19 epidemics

Authors: Nicholas G. Davies[1*], Petra Klepac[1^], Yang Liu[1^], Kiesha Prem[1], Mark Jit[1], CMMID COVID-19 working group, Rosalind M Eggo[1*]

The CMMID COVID-19 working group[1] is: Carl A B Pearson, Billy J Quilty, Adam J Kucharski, Hamish Gibbs, Samuel Clifford, Amy Gimma, Kevin van Zandvoort, James D Munday, Charlie Diamond, W John Edmunds, Rein MGJ Houben, Joel Hellewell, Timothy W Russell, Sam Abbott, Sebastian Funk, Nikos I Bosse, Fiona Sun, Stefan Flasche, Alicia Rosello & Christopher I Jarvis. Order of working group determined at random.

[1] Department of Infectious Disease Epidemiology, London School of Hygiene & Tropical Medicine, Keppel Street, WC1E 7HT

^ these authors contributed equally

* correspondence to Rosalind M Eggo r.eggo@lshtm.ac.uk or Nicholas G Davies nicholas.davies@lshtm.ac.uk

Abstract

The COVID-19 pandemic has shown a markedly low proportion of cases among children[1,23,4]. Age disparities in observed cases could be explained by children having lower susceptibility to infection, lower propensity to show clinical symptoms, or both. We evaluate these possibilities by fitting an age-structured mathematical model to epidemic data from six countries. We estimate that clinical symptoms occur in 25% (95% CrI: 19–32%) of infections in 10–19-year-olds, rising to 76% (68–82%) in over-70s, and that susceptibility to infection in under-20s is approximately half that of older adults. Accordingly, we find that interventions aimed at children may have a relatively small impact on total cases, particularly if the transmissibility of subclinical infections is low. The age-specific clinical fraction and susceptibility we have estimated has implications for the expected global burden of COVID-19 because of demographic differences across settings: in younger populations, the expected clinical attack rate would be lower, although it is likely that comorbidities in low-income countries will affect disease severity. Without effective control measures, regions with older populations may see disproportionally more clinical cases, particularly in the later stages of the pandemic.

Main

COVID-19 shows an increased number of cases and risk of severe disease with increasing age[5,6], a feature shared with the 2003 SARS epidemic [5]. Understanding the role of age in transmission and disease severity is critical for determining the likely impact of social-distancing interventions for decreasing transmission, especially those aimed at schools, and for estimating the expected global disease burden.

The age gradients in reported cases, observed from the earliest stages of the pandemic, could be generated by children having decreased susceptibility to infection, decreased

47 probability of showing disease on infection, or a combination of both. A summary of the main
48 findings, limitations and implications of the model for policy makers is shown in Table 1.
49

Background	The distribution of confirmed COVID-19 cases has shown strong age dependence, with notably few cases in children. This could be because younger ages are less susceptible to infection and/or are less prone to showing clinical symptoms when infected. We have used dynamic transmission models fitted to a range of available data on the age distribution of reported cases, and to studies that looked for subclinical infections amongst contacts, to estimate the age-specific susceptibility to SARS-CoV-2 infection, and the age-specific fraction of infections that develop clinical symptoms of COVID-19.
Main findings and limitations	We find that under-20s are roughly half as susceptible to infection as over-20s, and that 75% of infections are subclinical in 10–19-year olds, compared to 24% in 70+-year-olds. As with all modelling studies, further data generated during the epidemic could change our parameter estimates. Population mixing measured in contact surveys may not be representative of contact patterns made during the early phase of local epidemics. However, our estimates are consistent across countries and intervention contexts.
Policy implications	These results have implications for the likely effectiveness of school closures in mitigating SARS-CoV-2 transmission, in that these may be less effective than for other respiratory infections. They also have implications for the global expected burden of clinical cases; countries with a large number of children may need to account for decreased susceptibility and severity in burden projections.

50 Table 1. Policy Summary
51

52 Age-varying susceptibility to infection by SARS-CoV-2, where children may be less
53 susceptible to becoming infected on contact with an infectious person, would reduce cases
54 among children, and potentially lower transmission in the population overall. Decreased
55 susceptibility could result from immune cross-protection from other coronaviruses[8,910], or
56 possibly from non-specific protection resulting from recent infection by another respiratory
57 virus[11], which children experience more frequently than adults[12,13].
58

59 It is also possible that children may experience mild or no symptoms on infection more
60 frequently than adults. Such age-dependent variation in severity has been observed for other
61 respiratory virus infections[14], including SARS[14,15]. For COVID-19, there are indications of age
62 dependence in severity[8] and mortality[15] among reported cases[15], which could extend to

63 severity and likelihood of clinically reportable symptoms given infection. “Asymptomatic”
64 cases have no symptoms at all, and “paucisymptomatic” is sometimes used for those with
65 very mild symptoms that may not be noticed or reported, even though they occur. We call
66 these two types “subclinical”, which are more likely to remain undetected than clinically
67 apparent cases. If subclinical infections exhibit age dependence there would be lower
68 reported cases among children, but children could still be capable of transmitting the virus to
69 others, potentially at lower rates than individuals exhibiting clinical infections, as has been
70 shown for influenza[16].
71
72 Contact patterns and demographics affect the expected number of cases in each age group.
73 Children tend to make more social contacts than adults[17] and hence, all else equal,
74 contribute more to transmission than adults[18,19]. This is why school closures are considered
75 a key intervention for epidemics of respiratory infections[8], but the impact of school closure
76 depends on the role of children in transmission.
77
78 The particular context of SARS-CoV-2 emergence in Wuhan, China, could have resulted in a
79 skewed age distribution because early cases were in older adults[20], and assortative mixing
80 between adults could have reduced transmission to children in the very early stages of the
81 outbreak, with subsequent closure of schools on 12th January 2020 for the Lunar New Year
82 holiday potentially reinforcing this effect. Outside of China, COVID-19 outbreaks may have
83 been initially seeded by working-age travellers entering the country[21,22], producing a similar
84 excess of older individuals in early phases of local epidemics.
85
86 Determining the role of children in transmission using available data has important
87 implications for policies that aim to control transmission[23], especially through interrupting
88 child-driven transmission. Additionally, if the number of infections or cases depends strongly
89 on the role of children, countries with different age distributions could exhibit substantially
90 different epidemic profiles and overall impact of COVID-19 epidemics.

We used an age-stratified transmission model with heterogeneous contact rates between age groups to examine varying susceptibility to infection by age; varying clinical fraction by age; and no age variation in susceptibility or clinical fraction (see Methods). We generated model variants (**Fig 1a**) and fitted each to data sources from the epidemic in Wuhan: a time series of reported cases[1] and four snapshots of the age distribution of cases[124] (**Fig 1; Extended Data Figure 1**). We included the observed school closures, which decreased the school contacts of children in the model. We also estimated the effect of the Lunar New Year holiday period, and the travel and movement restrictions in Wuhan, on transmission (**Fig 1d**). We found that under each hypothesis, the basic reproduction number R_0 was 2.5-2.8 initially, was inflated 1.2–1.4-fold during the pre Lunar New Year holiday period, and then fell by 60–70% during restrictions in Wuhan (**Fig 1e**).

All model variants fitted the daily incident number of confirmed cases equally well (**Fig 1f**), but the model without age-varying susceptibility or clinical fraction could not reproduce the observed age distribution of cases, overestimating the number of cases in children and underestimating cases in older adults (**Fig 1g**). The other two fitted the observed age distribution of cases, but the model assuming no age variation in clinical fraction implied a large number of mild or asymptomatic infections among the elderly **(Fig 1h)**. Comparison using Deviance Information Criterion[6] (DIC) showed that age varying susceptibility (DIC: 697) and age-varying clinical fraction (DIC: 663) were preferred over the model with neither (DIC: 976).

In the model with age-varying susceptibility, 20% of infections occurred in over-70s, with half of these as clinical cases, and the other half as subclinical infections (**Fig 1h**). In the model with age-varying clinical fraction, 20% of infections occurred in over-70s, but less than a quarter of these were subclinical. Recent work has demonstrated an age-dependent severity

in hospitalised confirmed cases[25,26], which suggests that subclinical infection in older adults may be rare and supports the clinical fraction increasing with age.

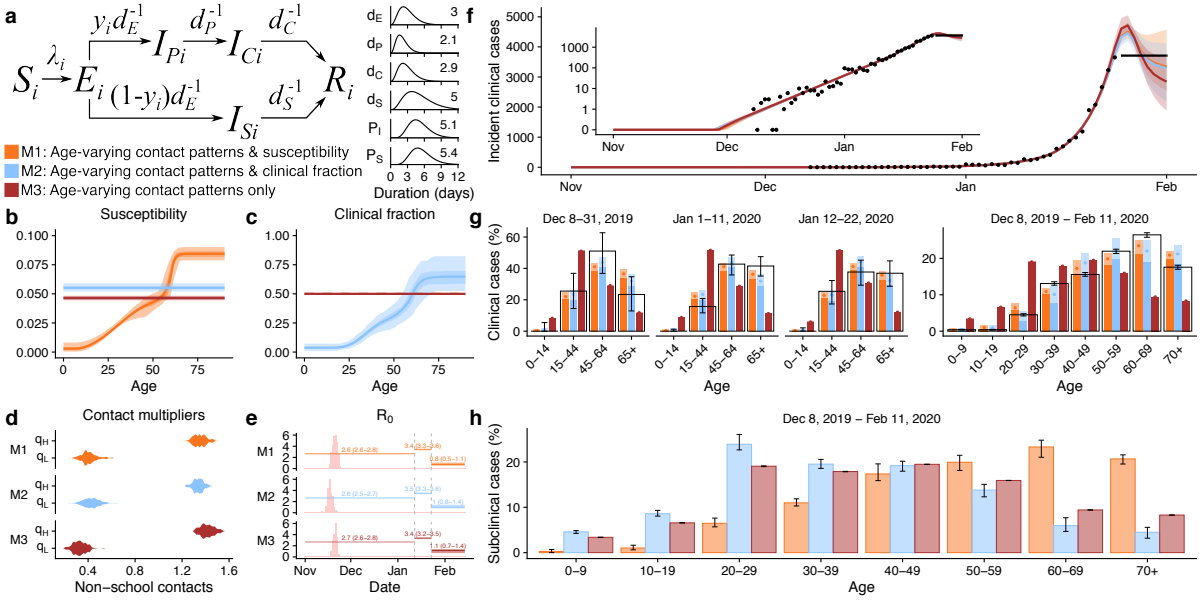

Fig. 1. Comparing the fit of different model variants to data from Wuhan City, China. (a) Model diagram showing duration of disease states in days, where *d* parameters represent the duration of time in each disease state, y_i is the fraction of infections that are clinical in age group *i*, λ_i is the force of infection in age group *i*, P_I is the incubation period and P_S is the serial interval (see Methods). **(b)** Susceptibility by age for the three models. Age-specific values were estimated for model 1 (orange). Susceptibility is defined as the probability of infection on contact with an infectious person. **(c)** Clinical fraction (y_i) by age for the three models. Age-specific values were estimated for model 2 (blue), and fixed at 0.5 for models 1 and 3. **(d)** Fitted contact multipliers for holiday (q_H) and restricted periods (q_L) for each model showed an increase in non-school contacts beginning on January 12th (start of Lunar New Year) and a decrease in contacts following restrictions on January 23rd. **(e)** Estimated R_0 values for each model. The red barplot shows the inferred window of spillover of infection. **(f)** Incident reported cases (black), and modelled incidence of reported clinical cases for the three models fitted to cases reported by China Centers for Disease Control (CCDC)[1] with onset on or before February 1st, 2020. Line marks mean and shaded window is the 95% highest density interval (HDI). **(g)** Age distribution of cases by onset date as fitted to the age distributions reported by Li et al[24] (first three panels) and CCDC[1] (fourth panel). Data are shown in the hollow bars, and model predictions in filled bars, where the dot marks the mean posterior estimate. **(h)** Implied distribution of subclinical cases by age for each model. Credible intervals on modelled values show the 95% HDIs; credible intervals on data for panels g and h show 95% HDIs for the proportion of cases in each age group.

It is possible that both age-varying susceptibility and age-varying clinical fraction contribute to some degree to the observed age patterns. To investigate this possibility, we fitted a model in which both susceptibility and clinical fraction varied by age, estimating these parameters across 32 settings in six countries. We fitted the stationary distribution of the next generation matrix to reproduce the locally-reported age distribution of cases compiled from a variety of sources **(Fig 2a)** and jointly fitted data from five recent studies giving information on infection rates and symptom severity across ages[25,27–30] (**Extended Data Figure 2**). We used setting-specific demographics, measured contact matrices where possible, and synthetic contact matrices otherwise (see Methods)[31]. The age-dependent clinical proportion was markedly lower in younger age groups in all regions **(Fig 2b),** with 25% (19–32%) of infections in 10–19-year-olds resulting in clinical cases, rising to 76% (68–82%) in adults over 70 in the consensus age distribution estimated across all regions; the age-specific susceptibility profile suggested that under-20s were half as susceptible to SARS-CoV-2 infection as over-20s (**Extended Data Table 1**). To determine whether this distribution was capable of reproducing epidemic dynamics, we fitted our dynamic model to the incidence of clinical cases in Beijing, Shanghai, South Korea and Italy (**Fig 2c; Extended Data Figure 3**). The consensus age-specific clinical fraction was largely capable of reproducing the age distribution of cases, although there are some outliers, for example in the 20–29 age group in South Korea. This could be the result of clustered transmission within a church group in this country[4]. The predicted age distribution of cases for Italy is also less skewed towards older adults than reported cases show, suggesting potential differences in age-specific testing in Italy[32]. Locally-estimated age-varying clinical fraction captured these patterns more precisely **(Fig. 2c)**.

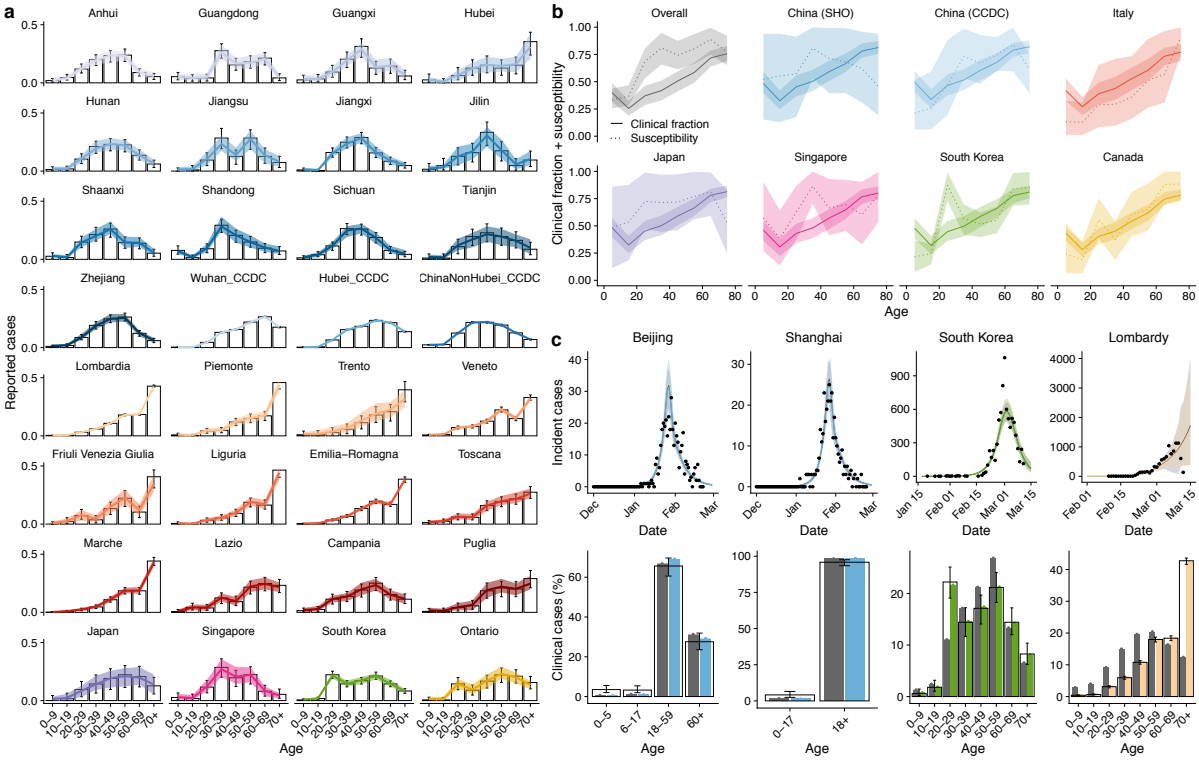

Fig 2. Estimating age-specific symptomatic rate from age-specific case counts for 6 countries. **(a)** Age-specific reported cases from 13 provinces of China, 12 regions of Italy, Japan, Singapore, South Korea, and Ontario, Canada. Hollow bars are data and colour is model fit with 95% HDI. **(b)** Fitted mean and 95% HDI for the age distribution in clinical fraction (solid lines) and age distribution of susceptibility (dashed lines) for all countries. The overall consensus fit is shown in grey. **(c)** Fitted incidence of confirmed cases and resulting age distribution of cases using either the consensus (grey) or country-specific (colour) age-specific clinical fraction from b.

School closures during epidemics[33,34] and pandemics[35,36] aim to decrease transmission amongst children[18], and may also have whole-population effects if children play a major role in transmission. The impact will depend on the fraction of the population that are children, the contacts they have with other age groups, their susceptibility to infection, and infectiousness if infected. Using schematic values for pandemic influenza[37] and our inferred values for COVID-19 **(Figure 3a)** we compared epidemics in three cities with very different demography: Milan (Italy, high median age), Birmingham (UK, intermediate median age), and Bulawayo (Zimbabwe, low median age) **(Fig 3b)**, using measured contact matrices for each country. There were many more clinical cases for COVID-19 than influenza in all cities (mean attack rate across three cities: 361 per 1000 for COVID-19 versus 23 per 1000 for influenza), with relatively more cases occurring in under-20s (68%) in the influenza-like

scenario compared to COVID-19 (17%) (**Fig 3c)**. More clinical cases were in older adults in Milan compared with the other cities, and a markedly younger age distribution was observed for clinical cases in Bulawayo. The age distribution of clinical cases depends on the demography and mixing in the region.

To explore the effect of school closure, we simulated 3 months of school closures with varying infectiousness of subclinical infections, at either 0%, 50% or 100% the infectiousness of clinical cases (**Fig 3d)**. For influenza- like infections we found that school closures decreased peak incidence by 17–35% across settings, and delayed the peak by 10-89 days across settings **(Fig 3e)**. For COVID-19 epidemics, the delay and decrease of the peak was smaller (9–18% decrease in peak incidence, 1–6 day delay in peak timing), especially in Bulawayo, which has the highest proportion of children **(Fig 3e)**. Because children have lower susceptibility and exhibit more subclinical cases for COVID-19, school closures were slightly more effective at reducing transmission of COVID-19 when the subclinical infectiousness was assumed to be higher (school closures were 37–53% more effective at reducing peak cases across settings for 100% versus 0% subclinical infectiousness) **(Fig 3f)**.

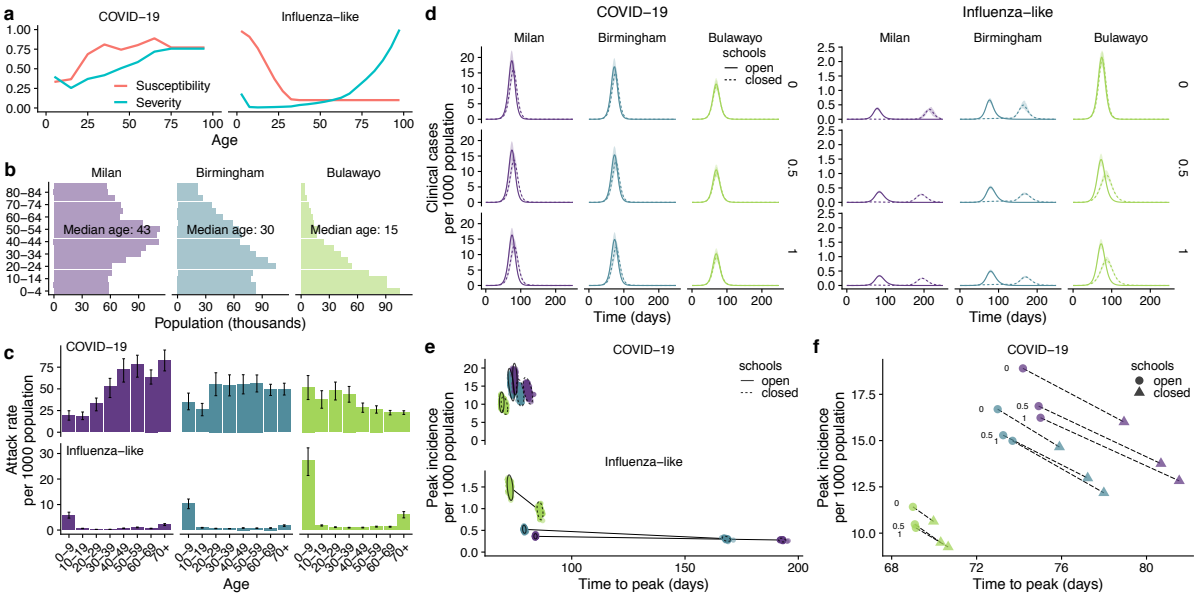

Fig. 3. Effect of school closure under different demographics and subclinical infectiousness. **(a)** Age dependence in clinical fraction (severity) and susceptibility to infection on contact for COVID-19, and for the influenza-like scenarios (simplified, based on ref. [37]) considered here. **(b)** Age structure for the 3 exemplar cities. **(c)** Age-specific attack rate for COVID-19 and influenza-like infections, assuming 50% subclinical infectiousness. **(d)** Daily incidence of clinical cases in exemplar cities for COVID-19 versus influenza-like infections. R_0 is fixed at 2.4. The rows show the impact of varying the infectiousness of subclinical infections to be 0%, 50%, or 100% as infectious as clinical cases while keeping R_0 fixed. **(e)** Change in peak timing and peak cases for the three cities, for either COVID-19 or influenza-like. **(f)** Change in median COVID-19 peak timing and peak cases for the three cities, depending on the infectiousness of subclinical infections.

Age dependence in susceptibility and clinical fraction has implications for the projected global burden of COVID-19. We simulated COVID-19 epidemics in 146 capital cities and found that the total expected number of clinical cases in an unmitigated epidemic varied between countries depending on the median age of the population, which is a proxy for the age structure of the population. The mean estimated basic reproduction number, R_0, did not substantially differ by median age (**Fig 4c**), because although there was a greater proportion of children the susceptibility of children was lower. We applied the same age-dependent clinical fraction to all countries, but the relationship between age and clinical symptoms may be different in different countries, perhaps because of a different distribution of comorbidities[38], or setting—specific comorbidities such as HIV[39]. If the relationship between

clinical fraction and age skews younger in low and lower-middle income countries, there would be higher clinical attack rates in these countries (**Extended Data Figure 4**).

The expected age distribution of cases shifted substantially during the epidemic, where in the early phase there were more cases in the central age group (20-59), and after the peak a higher proportion on cases in younger and older ages (**Fig 4d**). The size of the shift was higher in countries with higher median age, which impacts projections for likely healthcare burdens at different phases of the epidemic (**Fig 4e**), particularly because older individuals tend to have higher healthcare utilisation if infected[1].

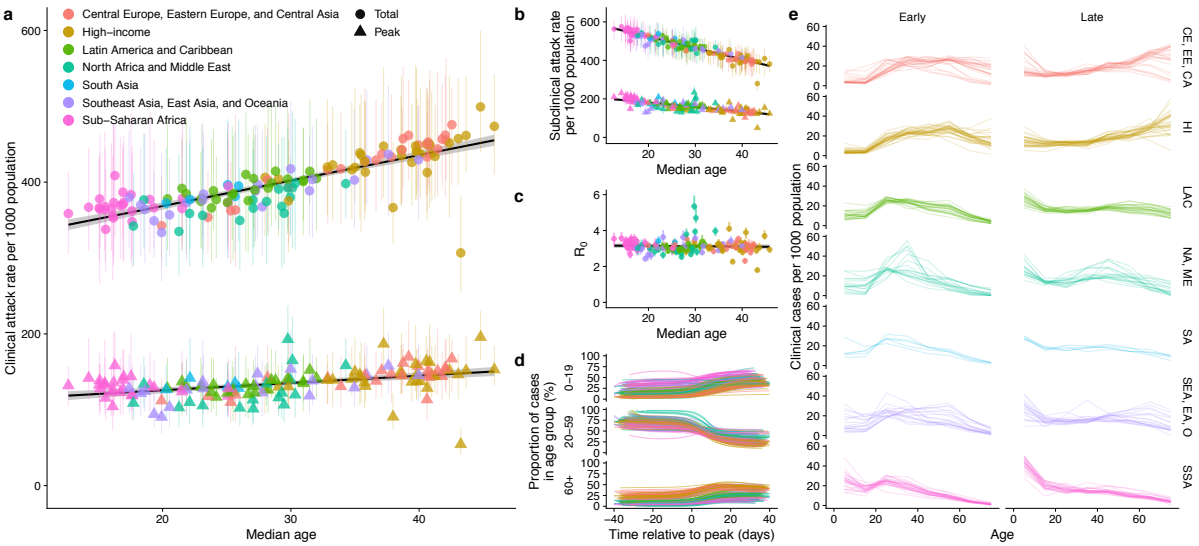

Fig. 4. Implications for global preparedness. (a) Expected clinical case attack rate (mean and 95% HDI), and peak in clinical case incidence for 146 countries in the Global Burden of Disease (GBD) country groupings[40] for an unmitigated epidemic. **(b)** Expected sub clinical case attack rate, and peak in subclinical cases. **(c)** Estimated basic reproduction number (R_0) in the capital city of each country assuming age-specific clinical fraction shown in Fig. 2b and 50% infectiousness of subclinically infected people. **(d)** Proportion of clinical cases in each age group at times relative to the peak of the epidemic. The 146 city epidemics were aligned at the peak, and colours mark the GBD groupings in a. **(e)** Age distribution of the first third and last third of clinical cases for 146 countries in GBD country groupings.

We have shown age dependence in susceptibility to infection and in the probability of displaying clinical symptoms of COVID-19, from around 20% in under 10s, to over 70% in older adults. For a number of other pathogens, there is evidence that children (except for the

very youngest) have lower rates of symptomatic disease[12] and mortality[26], so the variable age-specific clinical fraction for COVID-19 we find here fits with other studies. We have quantified the age-specific susceptibility from available data, and other study types will be needed to build the evidence base for the role of children, including serological surveys, and close follow up of infected households.

The age-specific distribution of clinical infection we have found is similar in shape (but larger in scale) to that generally assumed for pandemic influenza, but the age-specific susceptibility is inverted. These differences have a large effect on how effective school closures may be in limiting transmission, delaying the peak of expected cases, and decreasing the total and peak number of cases. For COVID-19, school closures are likely to be much less effective than for influenza-like infections.

It is critical to determine how infectious subclinical infections are compared to clinical infections in order to properly assess predicted burdens both with and without interventions. It is biologically plausible that milder cases are less transmissible, for example, because of an absence of cough[28,29], but direct evidence is limited[41] and viral load is high in both clinical and subclinical cases[30]. If those with subclinical infection are efficient transmitters of infection compared to those with clinical infections, the overall burden is higher than if they are not as infectious. At the same time, lower relative infectiousness would reduce the impact of interventions targeting younger ages, such as school closure. By analysing epidemic dynamics before and after school closures, or close follow up in household studies, it may be possible to estimate the infectiousness of subclinical infections, however this will rely on granular data by age and time.

A great deal of concern has been directed toward the expected burden of COVID-19 in low and middle income countries (LMIC), which have lower population median age than many high income countries. Our results show that these demographic differences, coupled with a

lower susceptibility and clinical fraction in younger ages, can result in proportionally fewer clinical cases than would be expected in higher-income countries with flatter demographic pyramids. This should not be interpreted as few cases in LMIC, because the projected epidemics are still very large, resulting in high numbers infected. Moreover, the particular relationships found between age, susceptibility, and clinical fraction are drawn from high and middle income countries and may reflect not only age, but also the increasing frequency of comorbidities with age. This relationship may therefore differ in LMIC for two key reasons: first, the distribution of non-communicable comorbid conditions—which are already known to increase the risk of severe disease from COVID-19[15] may be differently distributed by age, often occurring in younger age groups[40], along with other possible risk factors such as undernutrition[42]; and second, communicable comorbidities such as HIV[39], TB coinfection (which has been suggested to increase risk[43]), and others[44] may alter the distribution of severe outcomes by age. Observed severity and burden in LMIC may also be higher due to a lack of health system capacity for intensive treatment of severe cases.

There are some limitations to the study. While information drawn from the early stages of the epidemic is subject to uncertainty, age-specific information is drawn from several regions and countries, and clinical studies support the hypothesis presented here. We assumed that clinical cases are reported at a fixed fraction throughout the time period, although there may have been changes in reporting and testing practices that affected case ascertainment by age. We assumed that subclinical infections were less infectious than clinical infections, and tested the impact of this on our findings (**Extended Data Figures 5 and 6**) but were not able to estimate how infectious subclinical infections were. The sensitivity analyses showed very similar clinical fraction and susceptibility with age, and we demonstrated the effect of this parameter on school closure and global projections (**Fig. 3, Extended Data Figure 6**). We have used mixing matrices from the same country, but not the same location as the fitted data. We used contact matrices that combined physical and conversational contacts. We therefore implicitly assume that they are a good reflection of contact relevant for the

transmission of SARS-CoV-2. If fomite, or faecal-oral routes of transmission are important in transmission, these contact matrices may not be representative of transmission risk.

The role of age in transmission is critical to designing interventions aiming to decrease transmission in the population as a whole, and to projecting the expected global burden. Early evidence[25], including presented here, suggests that there is age dependence in susceptibility and in the risk of clinical symptoms following infection. Understanding if and by how much subclinical infections contribute to transmission has implications for predicted global burden and the impact of control interventions. This question must be resolved to effectively forecast and control COVID-19 epidemics.

Methods

Transmission model structure used in all analyses

We use an age-structured deterministic compartmental model (Fig. 1a, main text) stratified into 5-year age bands, with time approximated in discrete steps of 0.25 days. Compartments in the model are stratified by infection state (S, E, I_P, I_C, I_S, or R), age band, and the number of time steps remaining before transition to the next infection state. We assume that people are initially susceptible (S), and become exposed (E) after effective contact with an infectious person. After a latent period, exposed individuals either develop a clinical or subclinical infection; an exposed age-*i* individual develops a clinical infection with probability y_i, otherwise developing a subclinical infection. Clinical cases are preceded by a preclinical but infectious (I_P) state; from the preclinical state, individuals develop full symptoms and become clinically infected (I_C). Based on evidence for other respiratory infections[16] we assume that subclinical infections (I_S) are less infectious compared to preclinical and clinical infections, and that subclinical individuals remain in the community until they recover. We use 50% as a baseline for the relative infectiousness of individuals in the subclinical state, and test the impact of other values (**Extended Data Figs. 5 and 6**). Isolated and recovered individuals eventually enter the removed state (R); we assume these individuals are no longer infectious and are immune to reinfection.

The length of time individuals spend in states E, I_P, I_C, or I_S is distributed according to distributions d_E, d_P, d_C, or d_S, respectively (**Extended Data Table 2**). The force of infection for an individual in age group *i* at time *t* is

$$\lambda_{i,t} = u_i \sum_j c_{ij,t}(I_{Pj} + I_{Cj} + fI_{Sj})/N_j,$$

where u_i is the susceptibility to infection of an age-*i* individual, $c_{ij,t}$ is the number of age-*j* individuals contacted by an age-*i* individual per day at time *t*, *f* is the relative infectiousness of a subclinical case, and $(I_{Pj} + I_{Cj} + fI_{Sj})/N_j$ is the effective probability that a random age-*j*

individual is infectious. Contacts vary over time *t* depending upon the modelled impact of school closures and movement restrictions (see below).

To calculate the basic reproductive number, R_0, we define the next generation matrix as

$$NGM_{ij} = u_i c_{ij,t}(y_j E(d_P + d_C) + (1 - y_j) f E(d_S) \text{ .}$$

R_0 is the absolute value of the dominant eigenvalue of the next generation matrix.

We use the local age distribution for each city or region being modelled, and synthetic or measured contact matrices for mixing between age groups (**Extended Data Table 2**). The mixing matrices have four types of contacts: home, school, work and other contacts.

Comparing models by fitting to the Wuhan epidemic

We contrasted three models. In model 1, susceptibility varied by age ($u_i = u(i)$), but the proportion of exposed individuals who became clinical cases did not vary ($y_i = y$). In model 2, the clinical case probability varied by age ($y_i = y(i)$), but susceptibility did not ($u_i = u$). In model 3, there were no age-related differences in susceptibility or clinical fraction ($u_i = u$, and $y_i = y$). Susceptibility and clinical fraction curves were fitted using three control points for young, middle, and old age, interpolating between them with a half-cosine curve (see below for details).

We assumed that the initial outbreak in Wuhan was seeded by introducing one exposed individual per day of a randomly drawn age between A_{min} *and* A_{max} for 14 days starting on a day (t_{seed}) in November[30,31]. We used the age distribution of Wuhan City prefecture in 2016[45] and contact matrices measured in Shanghai[32] as a proxy for large cities in China. This contact matrix is stratified into school, home, work, and other contacts. We aggregated the last three categories into non-school contacts and estimated how components of the contact matrix changed early in the epidemic in response to major changes. Schools closed on

January 12th for the Lunar New Year holiday, so we decreased school contacts, but the holiday period may have changed non-school contacts, so we estimate this effect by inferring the change in non-school contact types, q_H. Large-scale restrictions started on January 23rd 2020 giving restrictions on travel and movement imposed by authorities, and we inferred the change in contact patterns during this period, q_L. Specifically:

$$c_{ij,t} = school(t) \cdot c_{ij|school} + other(t) \cdot c_{ij|other},$$

where

$$school(t) = \begin{cases} 1 & t < 12 \text{ January} \\ 0 & t \geq 12 \text{ January} \end{cases}$$

and

$$other(t) = \begin{cases} 1 & t < 12 \text{ January} \\ q_H & 12 \text{ January} \leq t < 23 \text{ January} \\ q_L & t \geq 23 \text{ January}. \end{cases}$$

We fitted the model to incident confirmed cases from the early phase of the epidemic in China (December 8, 2019-February 1, 2020) reported by China CDC[1]. During this period, the majority of cases were from Wuhan City, and we truncated the data after February 1st because there were more cases in other cities after this time. We jointly fitted the model to the age distribution of cases at 3 time windows (December 8, 2019 to January 22, 2020) reported by Li et al.[24] and a further time window (December 8, 2019 to February 11, 2020) reported by China CDC[1]. Because there was a large spike of incident cases reported on February 1 determined to have originated from the previous week, we amalgamated all cases from January 25 to February 1, including those in the large spike, into a single data point for the week. We assumed 10% of clinical cases were reported[19]. We used a Dirichlet distribution with a flat prior to obtain 95% HDIs for reported case data stratified by age group for display in figures.

We used Markov-chain Monte Carlo to jointly fit each hypothesis to the two sets of empirical observations from the epidemic in Wuhan City, China (**Supplementary Table 1**). We used a

negative binomial likelihood for incident cases and a Dirichlet-multinomial likelihood for the age distribution of cases, using the likelihood

$$L = \left(\prod_{k=1}^{K} NegBinom(C_k|size = 200, mean = c_k)\right)\left(\prod_{m=1}^{M} DirMultinom(A_m|\frac{200}{||a_m||}a_m)\right)$$

Above, C_k is the observed incidence on day k while c_k is the model-predicted incidence for day k, for each of K days. A_m is the observed age distribution for time period m (case counts for each age group) while a_m is the model-predicted age distribution for the same period, and $||a_m||$ is the total number of cases over all age groups in time period m, measured for M time periods. We set the precision of each distribution to 200 to capture additional uncertainty in data points that would not be captured with a Poisson or multinomial likelihood model.

For all Bayesian inference (i.e. shown in Figs. 1 and 2), we used differential evolution Markov chain Monte Carlo[46], first running numerical optimization to place starting values for each chain near the posterior mode. We then run 2000-3000 samples of burn-in, and generate at least 10,000 samples post-burn-in. Recovered posterior distributions, with prior distributions overlaid, are shown in **Extended Data Fig. 1**. We distinguished fitted models using Deviance Information Criterion (DIC)[47].

Analysis of the stationary age distribution of cases

To infer age-specific clinical fraction and susceptibility from reported case distributions, we assumed that reported cases follow the stationary distribution of cases reached in the early phase of an epidemic. Using our dynamic model would allow modelling any transient emphasis in the case distribution associated with the age of the individuals who seeded infection in a given region, but since the age of the true first cases is not generally known, we used the stationary distribution instead. Specifically, we used Bayesian inference to fit age-specific susceptibility and clinical fraction to the reported case distribution by first generating the expected case distribution k_i from (1) the age-specific susceptibility, u_i, (2) the

435 age-specific clinical fraction, y_i, (3) the measured or estimated contact matrix for the country,
436 and (4) the age structure of the country or region. We then used the likelihood

437 $$L = Multinom(c_i \,|k_i),$$
438
439 where c_i is the observed case distribution, when fitting to data from a single country or
440 region. When fitting to a combined set of regions and/or countries, we used the likelihood

441 $$L = \prod_{j=1}^{m} DirMultinom(c_{i,j} \,|sk_{i,j})^{w_j}$$

442 across countries $j \in \{1,2,\ldots,m\}$ with weights w_j such that $\prod_j \; w_j = 1$. We weighted[48] each of
443 the 13 provinces of China in our data set by 1/13, each of the 12 regions of Italy by 1/12, the
444 three reported case distributions from China CDC by 1/3, and data from South Korea,
445 Singapore, Japan and Ontario each by 1, then scaled all weights to multiply to 1.
446
447 The age-specific susceptibility u_i and age-specific clinical fraction y_i were estimated by
448 evaluating the expected case distribution c_i according to the likelihood functions given
449 above. It is not possible to identify both u_i and y_i from case data alone. Accordingly, we
450 inferred the age-specific clinical fraction, y_i from surveillance data from Italy reporting the
451 age-specific number of cases that were asymptomatic, paucisymptomatic, mild, severe, and
452 critical[29]. We assumed that asymptomatic and paucisymptomatic infections may be
453 underascertained relative to mild, severe, and critical cases, and therefore estimated an
454 "inflation factor" $z > 1$ giving the number of unascertained asymptomatic or
455 paucisymptomatic infections for each reported infection in these data. Accordingly, we
456 applied the likelihood penalty

457 $$P_L = \prod_i Beta\left(\frac{mild_i + sev_i + crit_i}{z(asymp_i + pauci_i) + mild_i + sev_i + crit_i}\middle|\alpha = 10000y_i, \beta = 10000(1 - y_i)\right)$$

458 when fitting y_i in order to constrain the relative shape of the clinical fraction curve by age.
459 Here, $mild_i$ is the number of mild cases reported in age group i, sev_i the number of severe
460 cases in age group i, etc. Therefore the age-specific clinical fraction reflected the proportion

of infections reported by Riccardo et al. as mild, critical, or severe, relative to an estimated proportion of asymptomatic and paucisymptomatic infections.

In order to estimate a value for the inflation factor *z* compatible with empirical data on the severity of infections, we applied a further likelihood penalty when estimating the consensus fit for clinical fraction and susceptibility in order to match information on age-specific susceptibility collected from recent contact-tracing studies[25,27,28,30]. A leave-one-out analysis showed that these additional data allowed the model fitting procedure to converge on a consistent profile for both u_i and y_i (**Extended Data Fig. 2**).

We extracted age-specific case data from the following sources. For provinces of China, we used age-specific case numbers reported by China CDC[1] as well as line list data compiled by the Shanghai Observer[49]. For regions of Italy, we used age-specific case numbers reported by the Istituto Superiore di Sanità on March 13, 2020[50]. For South Korea, we used the line list released by Kim et al. based on data from the Korea Centers for Disease Control and Prevention[22]. For Japan, we used the Open Covid Linelist[51,52]. For Singapore, we used Singapore Ministry of Health data compiled by Koh[21]. For Ontario, we used data compiled by the COVID-19 Canada Open Data Working Group[53].

To validate our line list analysis, we fitted the dynamic model to incidence data from Beijing, Shanghai, South Korea and Lombardy, Italy (**Extended Data Fig. 3**). We fixed the reporting rate for Beijing, Shanghai, South Korea, and Lombardy to 20%. Beijing and Shanghai incidence data were given by case onset, so we assumed no delay between reported and true case onsets. Incidence data for South Korea were given by the date of confirmation only; we assumed the reporting delay followed a gamma distribution with a 7-day mean. Incidence data for Italy were given separately for case onset and case confirmation, with only a subset of onset dates available; accordingly, we fit the proportion of confirmed cases with onset dates and the delay from onset to confirmation. We adjusted the size parameter

of the negative binomial distribution used to model case incidence to 10 to reflect greater variability among fewer data points for these countries than for Wuhan. Beijing and Shanghai were fitted jointly, with separate dates of introduction but the same fitted susceptibility, large-scale restriction date and large-scale restriction magnitude. South Korea and Italy were each fitted separately; we fitted a large-scale restriction date and magnitude for both South Korea and Italy.

For both the line list fitting and validation, we assumed that schools were closed in China, but remained open in South Korea, Japan, Italy, Singapore, and Canada, as schools were open for the majority of the period covered by the data in the latter five countries.

Quantifying the impact of school closure

To determine the impact in other cities with different demographic profiles we used the inferred parameters from our line list analysis to parameterise our transmission model for projections to other cities. We chose these to compare projections for a city with a high proportion of elderly individuals (Milan, Italy); a moderate-aged population (Birmingham, United Kingdom); and a city in a low-income country with a high proportion of young individuals (Bulawayo, Zimbabwe). For this analysis, we compared an outbreak of COVID-19, for which the burden and transmission is concentrated in relatively-older individuals, with an outbreak of pandemic influenza, for which the burden and transmission is concentrated in relatively-younger individuals. We assumed that immunity to influenza builds up over a person's lifetime, such that an individual's susceptibility to influenza infection plateaus at roughly age 35, and assumed that the severity of influenza infection is highest in the elderly and in children under 10 years old[37].

To model Milan, we used the age distribution of Milan in 2019[54] and a contact matrix measured in Italy in 2006[11]. To model Birmingham, we used the age distribution of Birmingham in 2018[55] and a contact matrix measured in the UK in 2006[11]. To model

Bulawayo, we used the age distribution of Bulawayo Province in 2012[56] and a contact matrix measured in Manicaland, Zimbabwe in 2013[57]. We assumed that the epidemic was seeded by two infectious individuals in a random age group per week for 5 weeks. We scaled the age-specific susceptibility u_i by setting the "target" basic reproductive number R_0 = 2.4, as a representative example. We also performed a sensitivity analysis where we scaled u_i to result in R_0 = 2.4 in Birmingham, and using the same setting for u_i in all three cities, so that the actual R_0 changed depending upon contact matrices and demographics used to model each city. This produced qualitatively similar results (**Extended Data Figure 7**).

We projected the impact of school closure by setting the contact multiplier for school contacts *school(t)* to 0. Complete removal of school contacts may overestimate the impact of school closures because of alternative contacts children make when out of school[58]. This will however give the maximum impact of school closures in the model to demonstrate the differences.

Projecting the global impact

To project the impact of COVID-19 outbreaks in global cities, we used mixing matrices from Prem et al.[31] and demographic structures for 2020 from World Population Prospects 2019 to simulate a COVID-19 outbreak in 146 global capital cities for which synthetic matrices, demographic structures and total populations were available. For simplicity, we assumed that capital cities followed the demographic structure of their respective countries and took the total population of each capital city from the R package *maps*. For each city, we scaled u_i to result in an average R_0 = 2.4 in Birmingham, UK, and used the same setting for u_i for all cities, so that the realised R_0 would change according to the contact matrices and demographics for each city. We simulated 20 outbreaks in each city, drawing the age-specific clinical fraction y_i from the posterior of the estimated overall clinical fraction from our line list analysis (Fig. 2), and analysed the time to the peak incidence of the epidemic, the peak clinical and subclinical incidence of infection, and the total number of clinical and

545 subclinical infections. We took the first third and the last third of clinical cases in each city to
546 compare the early and late stages of the epidemic.
547
548 **Contact matrices**
549 Wherever possible, we use measured contact matrices (**Supplementary Table 2**). We adapt
550 each of these mixing matrices, using 5-year age bands, to specific regions of the countries
551 they were measured in by reprocessing the original contact surveys with the population
552 demographics of the local regions. The contact matrices and demographics we used for
553 Figs. 1-3 of the main text are shown in **Extended Data Figure 8**.
554
555 The contact survey in Shanghai[59] allowed respondents to record both individual (one-on-
556 one) and group contacts, the latter with approximate ages. While individual contacts were
557 associated with a context (home, work, school, etc.) group contacts were not, and so we
558 assumed that all group contacts which involved individuals aged 0-19 occurred at school.
559 We also assumed that group contacts were lower intensity than individual contacts,
560 weighting group contacts by 50% relative to one-on-one contacts.
561
562 We assumed schools were closed during the epidemic in China (because schools closed for
563 the Lunar New Year holiday and remained closed), but open in Italy, Singapore, South
564 Korea, Japan, and Canada, because we used data from the early part of the epidemics in
565 those countries during which schools were open.
566
567 **Sensitivity analyses**
568 Since the infectiousness of subclinical individuals was not identifiable from data we have
569 available, in Figure 2 we adopted a baseline estimate of 50% relative to preclinical and
570 clinical individuals. In **Extended Data Figure 5**, we performed sensitivity analysis by
571 repeating our model runs with the alternative values for subclinical infectiousness between
572 0% and 100%. We did not find marked difference in the findings or estimates.

In Figure 2 we fitted the age distributions of cases in 6 countries jointly to findings from recent studies on the susceptibility of children. We tested the sensitivity of our findings to the findings of the other studies by conducting a leave one out sensitivity analysis. The results are given in **Extended Data Figure 2**, and we did not find major changes to the shape of the age-dependence in either susceptibility or clinical fraction.

In Fig. 3, we showed the epidemic in 3 cities with fixed R_0 at 2.4 to illustrate the impact that demographics alone have on the effectiveness of interventions. This means that higher rates of contact measured in surveys in in Milan and Bulawayo compared to Birmingham were not included. We also tested the sensitivity of findings on school closure for which we fix susceptibility u_i and therefore R_0 varies (**Extended Data Figure 7**). The conclusions regarding the relative effectiveness of school closures for COVID-19 versus influenza are similar.

In Fig. 4, we assumed that the age-specific clinical fraction was the same across all settings, but we tested the sensitivity of our projections (Figure 4) to the age-specific clinical fraction used in lower-income countries. However, a higher rate of comorbidities in lower-income countries could change the age-specific probability of developing clinical symptoms upon infection. To investigate this possibility, we construct a schematic alternative age-specific profile of clinical fraction by (1) increasing the age-specific probability of developing symptoms by 15% for individuals under the age of 20 and (2) shifting the age-specific clinical fraction for individual over the age of 20 by 10 years older (**Extended Data Figure 4**). We repeated the analyses with these functions and found increased burden in lower-income countries, that could exceed the burden of clinical cases in higher-income countries.

Finally, we repeated our projections for country-specific burdens of COVID-19 assuming different values for the relative infectiousness of subclinical infections. We found that this

had a relatively small impact on the relationship between median age and case burden across countries (**Extended Data Figure 6**).

Acknowledgements

We acknowledge the following for funding: NGD: National Institutes of Health Research (HPRU-2012-10096). PK, YL, KP, MJ: This research was partly funded by the Bill & Melinda Gates Foundation (INV-003174). PK: This work was funded in part by the Royal Society under award RP\EA\180004. YL, MJ: This research was partly funded by the National Institute for Health Research (NIHR) (16/137/109) using UK aid from the UK Government to support global health research. The views expressed in this publication are those of the author(s) and not necessarily those of the NIHR or the UK Department of Health and Social Care. RME: HDR UK (grant: MR/S003975/1).

The members of the CMMID COVID-19 working group and the funding they acknowledge are: Carl A B Pearson, Billy J Quilty (NIHR 16/137/109), Adam J Kucharski (Wellcome Trust grant: 206250/Z/17/Z), Hamish Gibbs (funded by the Department of Health and Social Care using UK Aid funding and is managed by the NIHR. The views expressed in this publication are those of the author(s) and not necessarily those of the Department of Health and SocialCare (ITCRZ 03010), Samuel Clifford (Wellcome Trust grant: 208812/Z/17/Z), Amy Gimma (Global Challenges Research Fund (GCRF) for the project "RECAP" managed through RCUK and ESRC (ES/P010873/1), Kevin van Zandvoort (supported by Elrha's Research for Health in Humanitarian Crises (R2HC) Programme, which aims to improve health outcomes by strengthening the evidence base for public health interventions in humanitarian crises. The R2HC programme is funded by the UK Government (DFID), the Wellcome Trust, and the UK National Institute for Health Research (NIHR), James D Munday (Wellcome Trust grant: 210758/Z/18/Z), Charlie Diamond (NIHR 16/137/109), W John Edmunds, Joel Hellewell (Wellcome Trust grant: 210758/Z/18/Z), Timothy W Russel (Wellcome Trust grant: 206250/Z/17/Z), Sam Abbott (Wellcome Trust grant: 210758/Z/18/Z), Sebastian Funk (Wellcome Trust grant: 210758/Z/18/Z), Nikos I Bosse, Fiona Sun (NIHR EPIC grant 16/137/109), Stefan Flasche (Wellcome Trust grant: 208812/Z/17/Z), Alicia Rosello (NIHR grant: PR-OD-1017-20002), Christopher I Jarvis (Global Challenges Research Fund (GCRF) project 'RECAP' managed through RCUK and ESRC (ES/P010873/1)), RMGJH (European Research Commission Starting Grant: #757699).

Author contributions

RME conceived the study. NGD and RME designed the model with PK, and YL, KP and MJ providing input. NGD designed the software and inference framework and implemented the model. YL processed the data. NGD and RME wrote the first draft of the manuscript. All authors interpreted the results, contributed to writing, and approved the final version for submission.

Data Availability and Code Availability

The data used for fitting are publicly available, but will also be made available with the code in the github repository for the project at https://github.com/nicholasdavies/covid-age. Contact matrix data are available at zenodo[21,22].

Competing interests

The authors have no competing interests.

Additional information

Supplementary Information is available for this paper. Correspondence and requests for materials should be addressed to Rosalind M Eggo or Nicholas G Davies at r.eggo@lshtm.ac.uk or nicholas.davies@lshtm.ac.uk

References

1. Zhang. The epidemiological characteristics of an outbreak of 2019 novel coronavirus diseases (COVID-19) in China. *Chin. J. Epidemiol.* **41**, 145–151 (20200217).
2. Sun, K., Chen, J. & Viboud, C. Early epidemiological analysis of the coronavirus disease 2019 outbreak based on crowdsourced data: a population-level observational study. *Lancet Digit. Health* S2589750020300261 (2020) doi:10.1016/S2589-7500(20)30026-1.
3. D, C. *et al.* The early phase of the COVID-19 outbreak in Lombardy, Italy. *ArXiv200309320 Q-Bio* (2020).
4. Shim, E., Tariq, A., Choi, W., Lee, Y. & Chowell, G. Transmission potential and severity of COVID-19 in South Korea. *Int. J. Infect. Dis.* S1201971220301508 (2020) doi:10.1016/j.ijid.2020.03.031.
5. Dong, Y. *et al.* Epidemiological Characteristics of 2143 Pediatric Patients With 2019 Coronavirus Disease in China. *Pediatrics* e20200702 (2020) doi:10.1542/peds.2020-0702.
6. Zhao, X. *et al. Incidence, clinical characteristics and prognostic factor of patients with COVID-19: a systematic review and meta-analysis*. http://medrxiv.org/lookup/doi/10.1101/2020.03.17.20037572 (2020) doi:10.1101/2020.03.17.20037572.
7. Anderson, R. M. *et al.* Epidemiology, transmission dynamics and control of SARS: the 2002–2003 epidemic. *Philos. Trans. R. Soc. Lond. B. Biol. Sci.* **359**, 1091–1105 (2004).
8. Nickbakhsh, S. *et al.* Epidemiology of Seasonal Coronaviruses: Establishing the Context for the Emergence of Coronavirus Disease 2019. *J. Infect. Dis.* jiaa185 (2020) doi:10.1093/infdis/jiaa185.

9. Kissler, S. M., Tedijanto, C., Goldstein, E., Grad, Y. H. & Lipsitch, M. Projecting the transmission dynamics of SARS-CoV-2 through the postpandemic period. *Science* eabb5793 (2020) doi:10.1126/science.abb5793.
10. Huang, A. T. *et al. A systematic review of antibody mediated immunity to coronaviruses: antibody kinetics, correlates of protection, and association of antibody responses with severity of disease*. http://medrxiv.org/lookup/doi/10.1101/2020.04.14.20065771 (2020) doi:10.1101/2020.04.14.20065771.
11. Cowling, B. J. *et al.* Increased Risk of Noninfluenza Respiratory Virus Infections Associated With Receipt of Inactivated Influenza Vaccine. *Clin. Infect. Dis.* **54**, 1778–1783 (2012).
12. Tsagarakis, N. J. *et al.* Age-related prevalence of common upper respiratory pathogens, based on the application of the FilmArray Respiratory panel in a tertiary hospital in Greece: *Medicine (Baltimore)* **97**, e10903 (2018).
13. Common cold. *nhs.uk* https://www.nhs.uk/conditions/common-cold/ (2017).
14. Galanti, M. *et al.* Rates of asymptomatic respiratory virus infection across age groups. *Epidemiol. Infect.* **147**, e176 (2019).
15. Zhou, F. *et al.* Clinical course and risk factors for mortality of adult inpatients with COVID-19 in Wuhan, China: a retrospective cohort study. *The Lancet* S0140673620305663 (2020) doi:10.1016/S0140-6736(20)30566-3.
16. Van Kerckhove, K., Hens, N., Edmunds, W. J. & Eames, K. T. D. The Impact of Illness on Social Networks: Implications for Transmission and Control of Influenza. *Am. J. Epidemiol.* **178**, 1655–1662 (2013).
17. Mossong, J. *et al.* Social Contacts and Mixing Patterns Relevant to the Spread of Infectious Diseases. *PLOS Med.* **5**, e74 (2008).
18. Cauchemez, S., Valleron, A.-J., Boëlle, P.-Y., Flahault, A. & Ferguson, N. M. Estimating the impact of school closure on influenza transmission from Sentinel data. *Nature* **452**, 750–754 (2008).
19. Eames, K. T. D., Tilston, N. L., Brooks-Pollock, E. & Edmunds, W. J. Measured Dynamic Social Contact Patterns Explain the Spread of H1N1v Influenza. *PLoS Comput. Biol.* **8**, e1002425 (2012).

20. Huang, C. *et al.* Clinical features of patients infected with 2019 novel coronavirus in Wuhan, China. *The Lancet* **395**, 497–506 (2020).
21. Koh, A. Singapore COVID-19 Cases. http://alexkoh.net/covid19/.
22. Data Science for COVID-19 (DS4C). https://kaggle.com/kimjihoo/coronavirusdataset.
23. Lipsitch, M., Swerdlow, D. L. & Finelli, L. Defining the Epidemiology of Covid-19 — Studies Needed. *N. Engl. J. Med.* **0**, null (2020).
24. Li, Q. *et al.* Early Transmission Dynamics in Wuhan, China, of Novel Coronavirus–Infected Pneumonia. *N. Engl. J. Med.* NEJMoa2001316 (2020) doi:10.1056/NEJMoa2001316.
25. Bi, Q. *et al. Epidemiology and Transmission of COVID-19 in Shenzhen China: Analysis of 391 cases and 1,286 of their close contacts*. http://medrxiv.org/lookup/doi/10.1101/2020.03.03.20028423 (2020) doi:10.1101/2020.03.03.20028423.
26. Yang, Y. *et al. Epidemiological and clinical features of the 2019 novel coronavirus outbreak in China*. http://medrxiv.org/lookup/doi/10.1101/2020.02.10.20021675 (2020) doi:10.1101/2020.02.10.20021675.
27. Zhang, J. *et al.* Age profile of susceptibility, mixing, and social distancing shape the dynamics of the novel coronavirus disease 2019 outbreak in China. (2020) doi:10.1101/2020.03.19.20039107.
28. Gudbjartsson, D. F. *et al.* Spread of SARS-CoV-2 in the Icelandic Population. *N. Engl. J. Med.* NEJMoa2006100 (2020) doi:10.1056/NEJMoa2006100.
29. Riccardo, F. *et al. Epidemiological characteristics of COVID-19 cases in Italy and estimates of the reproductive numbers one month into the epidemic*. http://medrxiv.org/lookup/doi/10.1101/2020.04.08.20056861 (2020) doi:10.1101/2020.04.08.20056861.
30. Lavezzo, E. *et al.* Suppression of COVID-19 outbreak in the municipality of Vo, Italy. (2020) doi:10.1101/2020.04.17.20053157.
31. Prem, K., Cook, A. R. & Jit, M. Projecting social contact matrices in 152 countries using contact surveys and demographic data. *PLOS Comput. Biol.* **13**, e1005697 (2017).
32. Onder, G., Rezza, G. & Brusaferro, S. Case-Fatality Rate and Characteristics of Patients Dying in Relation to COVID-19 in Italy. *JAMA* (2020) doi:10.1001/jama.2020.4683.

739 33. Chan, K. P. Control of Severe Acute Respiratory Syndrome in Singapore. *Environ. Health Prev.*
740 *Med.* **10**, 255–259 (2005).
741 34. Lau, J. T. F. Monitoring community responses to the SARS epidemic in Hong Kong: from day 10
742 to day 62. *J. Epidemiol. Community Health* **57**, 864–870 (2003).
743 35. Cauchemez, S. *et al.* School closures during the 2009 influenza pandemic: national and local
744 experiences. *BMC Infect. Dis.* **14**, 207 (2014).
745 36. Cauchemez, S. *et al.* Closure of schools during an influenza pandemic. *Lancet Infect. Dis.* **9**,
746 473–481 (2009).
747 37. Greer, A. L., Tuite, A. & Fisman, D. N. Age, influenza pandemics and disease dynamics.
748 *Epidemiol. Infect.* **138**, 1542–1549 (2010).
749 38. Clark, A. *et al. How many are at increased risk of severe COVID-19 disease? Rapid global,*
750 *regional and national estimates for 2020*.
751 http://medrxiv.org/lookup/doi/10.1101/2020.04.18.20064774 (2020)
752 doi:10.1101/2020.04.18.20064774.
753 39. Cohen, C. *et al.* Severe Influenza-associated Respiratory Infection in High HIV Prevalence
754 Setting, South Africa, 2009–2011. *Emerg. Infect. Dis.* **19**, (2013).
755 40. IHME. Global Burden of Disease. http://www.healthdata.org/gbd.
756 41. Williams, C. M. *et al.* Exhaled Mycobacterium tuberculosis output and detection of subclinical
757 disease by face-mask sampling: prospective observational studies. *Lancet Infect. Dis.*
758 S1473309919307078 (2020) doi:10.1016/S1473-3099(19)30707-8.
759 42. Murray, J. *et al.* Determining the Provincial and National Burden of Influenza-Associated Severe
760 Acute Respiratory Illness in South Africa Using a Rapid Assessment Methodology. *PLOS ONE*
761 **10**, e0132078 (2015).
762 43. Liu, Y. *et al. Active or latent tuberculosis increases susceptibility to COVID-19 and disease*
763 *severity*. http://medrxiv.org/lookup/doi/10.1101/2020.03.10.20033795 (2020)
764 doi:10.1101/2020.03.10.20033795.
765 44. Cohen, A. L. *et al.* Potential Impact of Co-Infections and Co-Morbidities Prevalent in Africa on
766 Influenza Severity and Frequency: A Systematic Review. *PLOS ONE* **10**, e0128580 (2015).
767 45. National Bureau of Statistics. China Statistical Year Book. (2005-2018).
768 http://www.stats.gov.cn/tjsj/ndsj/.

769 46. Braak, C. J. F. T. A Markov Chain Monte Carlo version of the genetic algorithm Differential
770 Evolution: easy Bayesian computing for real parameter spaces. *Stat. Comput.* **16**, 239–249
771 (2006).
772 47. Spiegelhalter, D. J., Best, N. G., Carlin, B. P. & van der Linde, A. Bayesian measures of model
773 complexity and fit. *J. R. Stat. Soc. Ser. B Stat. Methodol.* **64**, 583–639 (2002).
774 48. Varin, C., Reid, N. & Firth, D. An overview of composite likelihood methods. *Stat. Sin.* **21**, (2011).
775 49. Observer, S. Shanghai Observer. COVID-2019 Linelist.
776 http://data.shobserver.com/www/datadetail.html?contId=1000895.
777 50. Epicentro. *Bolletino Sorveglianza Integrata COVID-19 12 Marzo 2020 Appendix*.
778 https://www.epicentro.iss.it/coronavirus/bollettino/Bolletino-sorveglianza-integrata-COVID-19_12-
779 marzo-2020_appendix.pdf.
780 51. COVID19_2020_open_line_list.
781 https://docs.google.com/spreadsheets/d/1itaohdPiAeniCXNlntNztZ_oRvjh0HsGuJXUJWET008/e
782 dit?usp=sharing.
783 52. Xu, B. *et al.* Open access epidemiological data from the COVID-19 outbreak. *Lancet Infect. Dis.*
784 S1473309920301195 (2020) doi:10.1016/S1473-3099(20)30119-5.
785 53. COVID-19 in Canada. https://art-bd.shinyapps.io/covid19canada/.
786 54. Milano (Metropolitan City, Italy) - Population Statistics, Charts, Map and Location.
787 http://citypopulation.info/en/italy/admin/lombardia/015__milano/.
788 55. Age breakdown of the population of Birmingham - Office for National Statistics.
789 https://www.ons.gov.uk/aboutus/transparencyandgovernance/freedomofinformationfoi/agebreakd
790 ownofthepopulationofbirmingham.
791 56. Bulawayo (City, Zimbabwe) - Population Statistics, Charts, Map and Location.
792 http://citypopulation.info/php/zimbabwe-admin.php?adm1id=A.
793 57. Melegaro, A. *et al.* Social Contact Structures and Time Use Patterns in the Manicaland Province
794 of Zimbabwe. *PLOS ONE* **12**, e0170459 (2017).
795 58. Kucharski, A. J., Conlan, A. J. K. & Eames, K. T. D. School's Out: Seasonal Variation in the
796 Movement Patterns of School Children. *PLOS ONE* **10**, e0128070 (2015).
797 59. Zhang, J. *et al.* Patterns of human social contact and contact with animals in Shanghai, China.
798 *Sci. Rep.* **9**, 1–11 (2019).

799

Extended Data

Age-dependent effects in the transmission and control of COVID-19 epidemics

Authors: Nicholas G. Davies[1*], Petra Klepac[1^], Yang Liu[1^], Kiesha Prem[1], Mark Jit[1], CMMID COVID-19 working group, Rosalind M Eggo[1*]

The CMMID COVID-19 working group[1] is: Carl A B Pearson, Billy J Quilty, Adam J Kucharski, Hamish Gibbs, Samuel Clifford, Amy Gimma, Kevin van Zandvoort, James D Munday, Charlie Diamond, W John Edmunds, Rein MGJ Houben, Joel Hellewell, Timothy W Russell, Sam Abbott, Sebastian Funk, Nikos I Bosse, Fiona Sun, Stefan Flasche, Alicia Rosello & Christopher I Jarvis. Order of working group determined at random.

[1] Department of Infectious Disease Epidemiology, London School of Hygiene & Tropical Medicine, Keppel Street, WC1E 7HT
^ these authors contributed equally
* correspondence to Rosalind M Eggo r.eggo@lshtm.ac.uk or Nicholas G Davies nicholas.davies@lshtm.ac.uk

Parameter	*Age Group*	*Mean*	*Quantile 2.5%*	*Quantile 25%*	*Quantile 50%*	*Quantile 75%*	*Quantile 97.5%*
Susceptibility	0-9	0.33	0.25	0.3	0.33	0.36	0.43
Susceptibility	10-19	0.37	0.28	0.33	0.37	0.4	0.47
Susceptibility	20-29	0.69	0.54	0.64	0.69	0.74	0.82
Susceptibility	30-39	0.81	0.65	0.76	0.81	0.86	0.95
Susceptibility	40-49	0.74	0.59	0.7	0.75	0.79	0.86
Susceptibility	50-59	0.8	0.65	0.76	0.81	0.85	0.93
Susceptibility	60-69	0.89	0.72	0.85	0.9	0.94	0.99
Susceptibility	70+	0.77	0.62	0.72	0.78	0.82	0.9
Clinical fraction	0-9	0.4	0.31	0.36	0.4	0.44	0.48
Clinical fraction	10-19	0.25	0.19	0.23	0.25	0.29	0.32
Clinical fraction	20-29	0.37	0.28	0.33	0.37	0.41	0.46
Clinical fraction	30-39	0.42	0.33	0.38	0.42	0.46	0.51
Clinical fraction	40-49	0.51	0.41	0.47	0.51	0.55	0.6
Clinical fraction	50-59	0.59	0.48	0.55	0.59	0.62	0.67
Clinical fraction	60-69	0.72	0.63	0.69	0.72	0.75	0.79
Clinical fraction	70+	0.76	0.68	0.73	0.76	0.79	0.82

Extended Data Table 1. Posterior estimates for the consensus susceptibility and clinical fraction from 6 countries. Note that susceptibility is a relative measure.

Parameter	Description	Applies in fits	Value	Reference
d_E	Incubation period (E to I_P and E to I_S; days)	All	$\sim gamma(\mu = 3.0, k = 4)$	Derived from[1] [2]
d_P	Duration of preclinical infectiousness (days)	All	$\sim gamma(\mu = 2.1, k = 4)$	Derived from[2]
d_C	Duration of clinical infectiousness (I_C to R; days)	All	$\sim gamma(\mu = 2.9, k = 4)$	[3]
d_S	Duration of subclinical infectiousness (days)	All	$\sim gamma(\mu = 5, k = 4)$	Assumed
u_i	Susceptibility for age group *i*	Varies by age in Wuhan hypothesis 2, otherwise all ages equal	Estimated	
y_i	Probability of clinical infection for age group *i*	Varies by age in Wuhan hypothesis 3, otherwise all ages equal	Either fixed (50%) or estimated	[4]
f	Relative infectiousness of subclinical cases	All	50% (0% and 100% in sensitivity analysis)	Assumed
c_{ij}	Number of age-*j* individuals contacted by an age-*i* individual per day	All	Country-specific contact matrix (sensitivity analysis using synthetic matrices[19])	China[32]; UK[7]; Zimbabwe[34]
N_i	Number of age-*i* individuals	All	Demographic data	[5]
Δt	Time step for discrete-time simulation	All	0.25 days	
A_{min}, A_{max}	Age range of seed cases	Wuhan	Estimated	
t_{seed}	Day upon which seeding of infections starts	All	Estimated	
q_H	Relative change in non-school contacts during lunar new year holidays	Wuhan	Estimated	
q_L	Relative change in non-school contacts following large-scale restrictions	Wuhan, South Korea, Shanghai, Beijing, Italy	Estimated	
t_L	Day upon which large-scale restrictions start	Wuhan, South Korea, Shanghai, Beijing, Italy	Fixed to January 23 for Wuhan; estimated for other settings	

Extended Data Table 2. Model parameters.

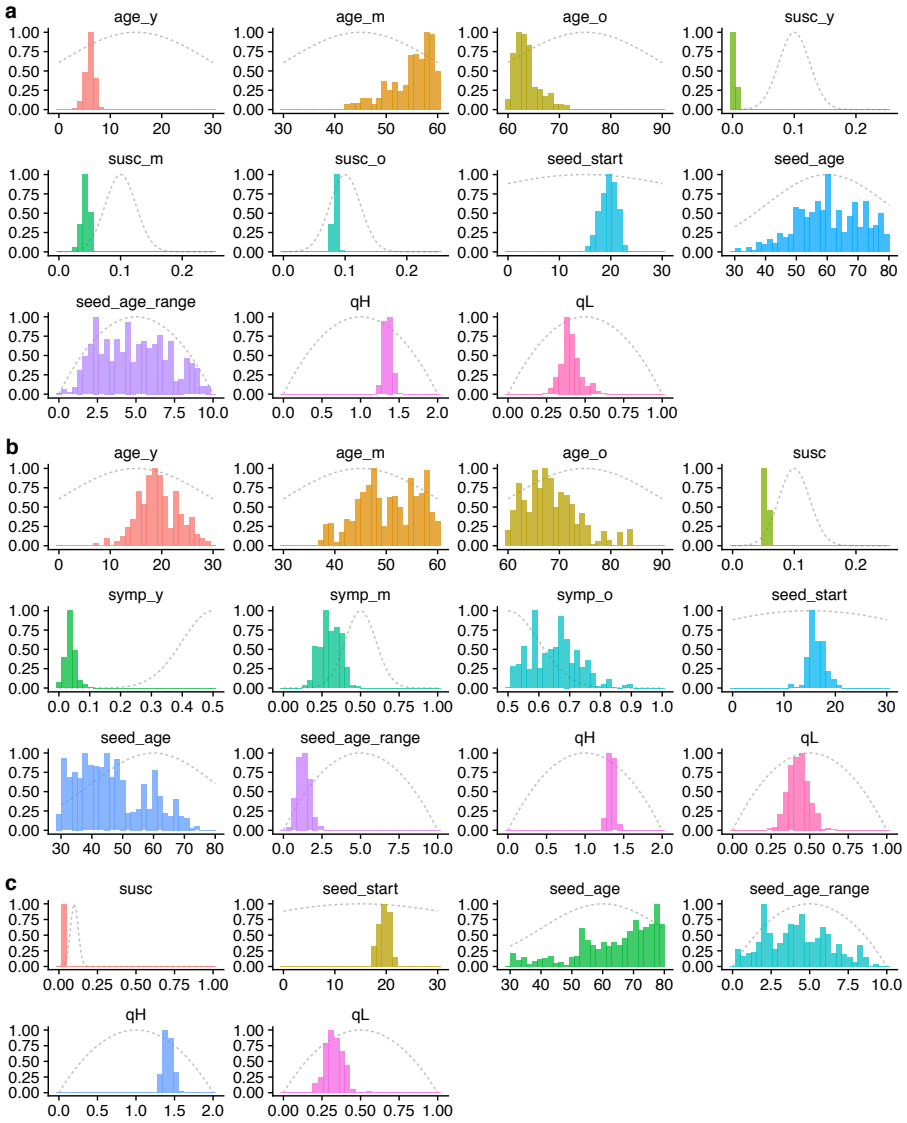

Extended Data Figure 1. Prior distributions (grey dotted lines) and posterior distributions (coloured histograms) for model parameters fitting to the early epidemic in Wuhan (Fig. 1, main text); seed_start is measured in days after November 1st, 2019. **(a)** Model 1 (age-varying contact patterns and susceptibility); **(b)** Model 2 (age-varying contact patterns and clinical fraction); **(c)** Model 3 (age-varying contact patterns only). See also Supplementary Table 3.

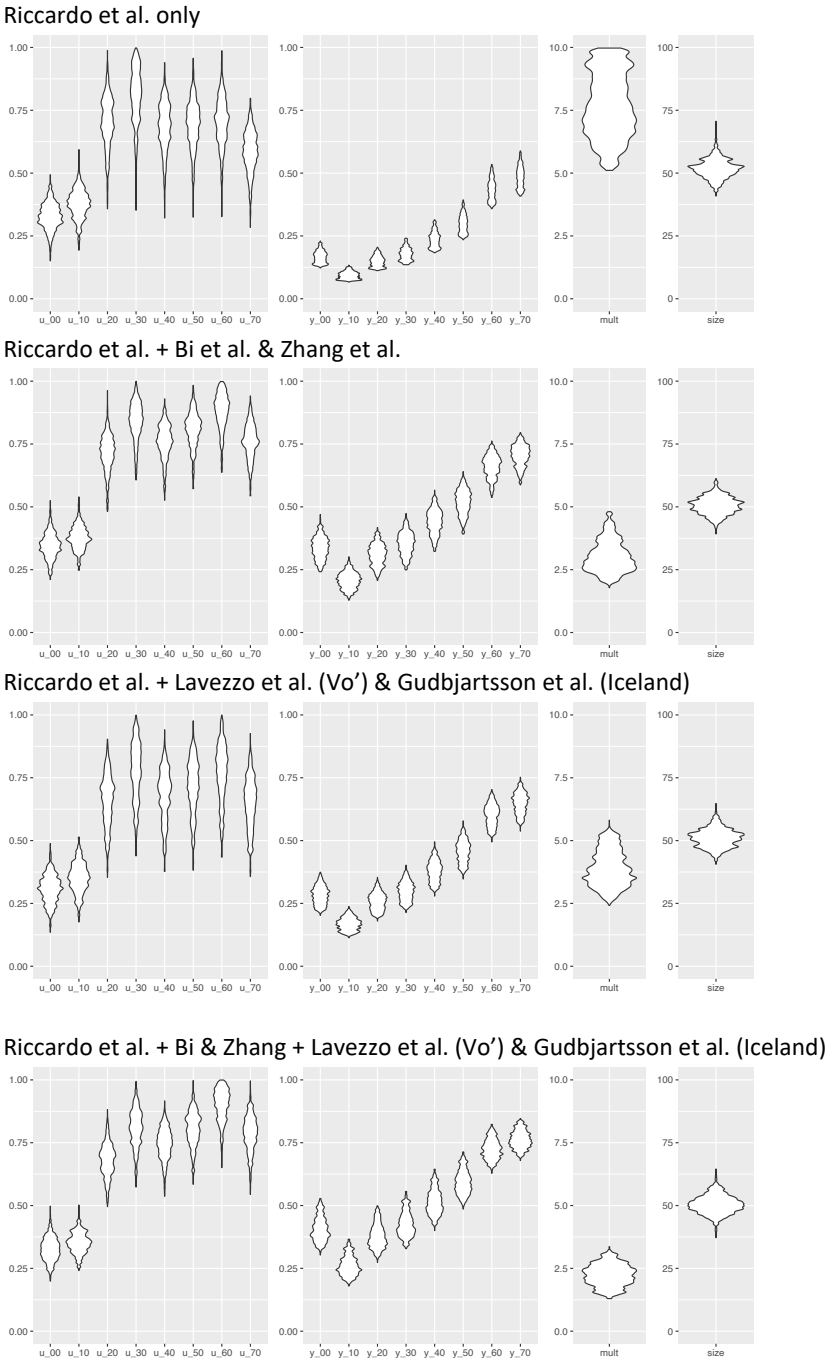

Extended Data Figure 2. Analysis showing how the inferred age-varying susceptibility (first column) and age-varying clinical fraction (second column) depend upon the additional data sources used.

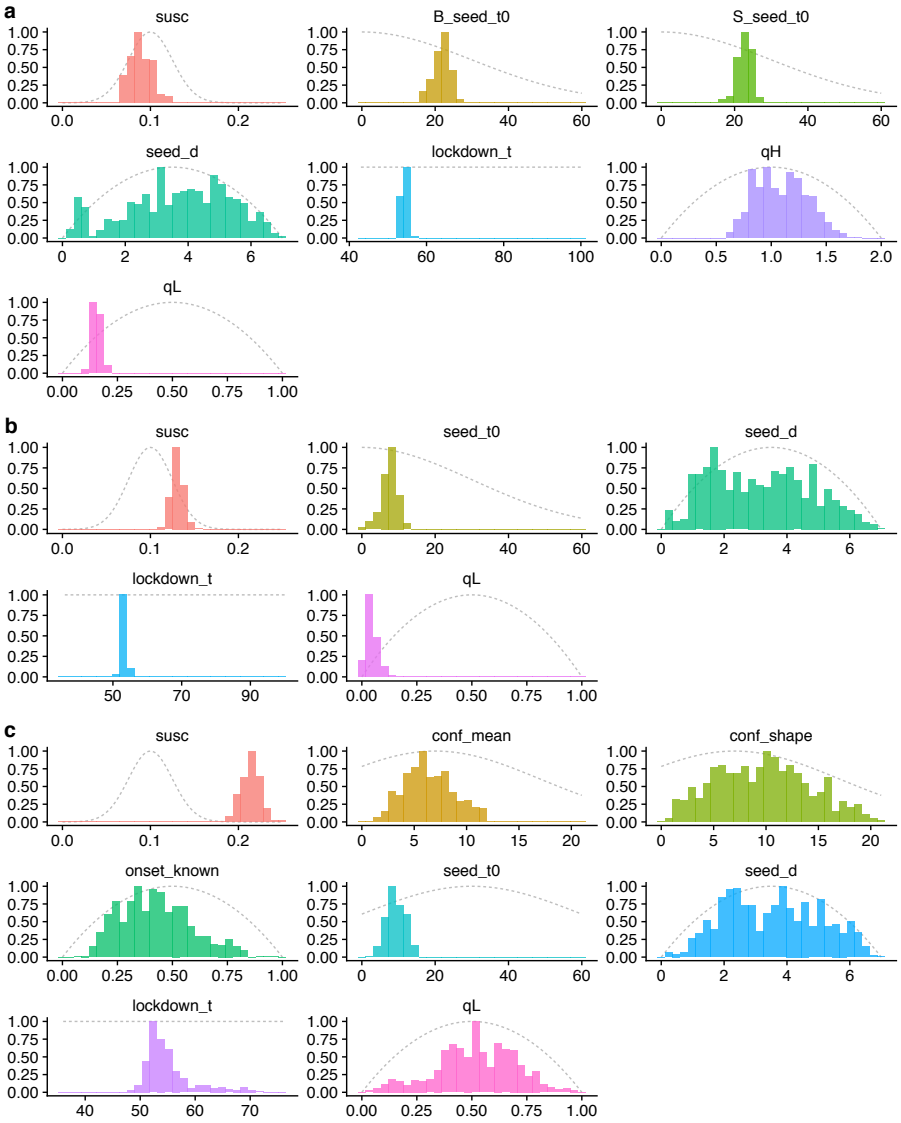

Extended Data Figure 3. Prior and posterior distributions for the epidemics in **(a)** Beijing and Shanghai, **(b)** South Korea and **(c)** Lombardy using the "consensus" fit for age-specific clinical fraction and assuming subclinical infections are 50% as infectious as clinical infections (see Fig. 2c, main text). For **(a),** times are in days after December 1st, 2019; for **(b)** and **(c)**, times are in days after January 1st, 2019. Note, seed_d is the inferred duration of the seeding event. See also Supplementary Table 3.

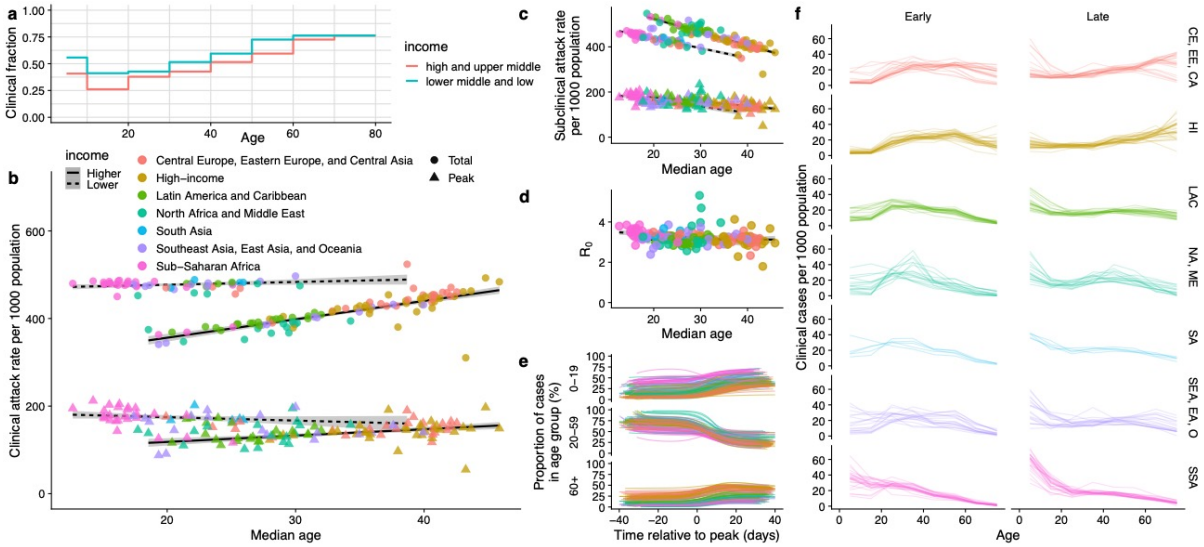

Extended Data Figure 4. Global projections assuming greater severity in lower-income countries. **(a)** Schematic age-specific clinical fraction for higher-income and lower-income countries. **(b-f)** Illustrative results of the projections for 146 capital cities assuming a higher age-varying clinical fraction in lower-income countries. See Fig. 4 (main text) for details.

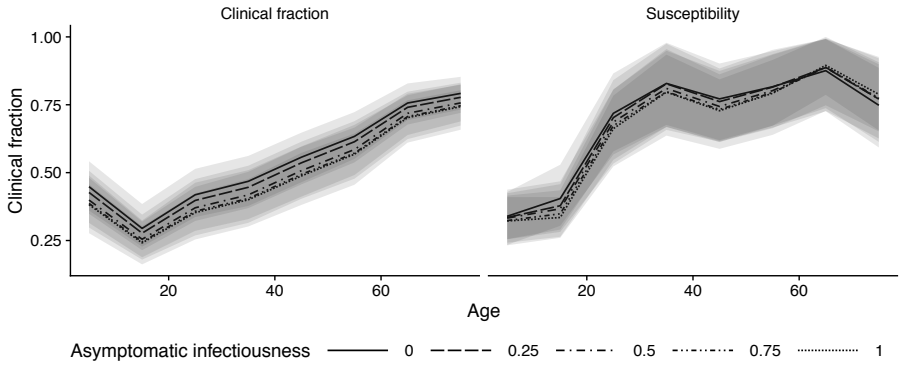

Extended Data Figure 5. Consensus age-specific clinical fraction and susceptibility, assuming subclinical infections are 0%, 25%, 50%, 75%, or 100% as infectious as clinical infections.

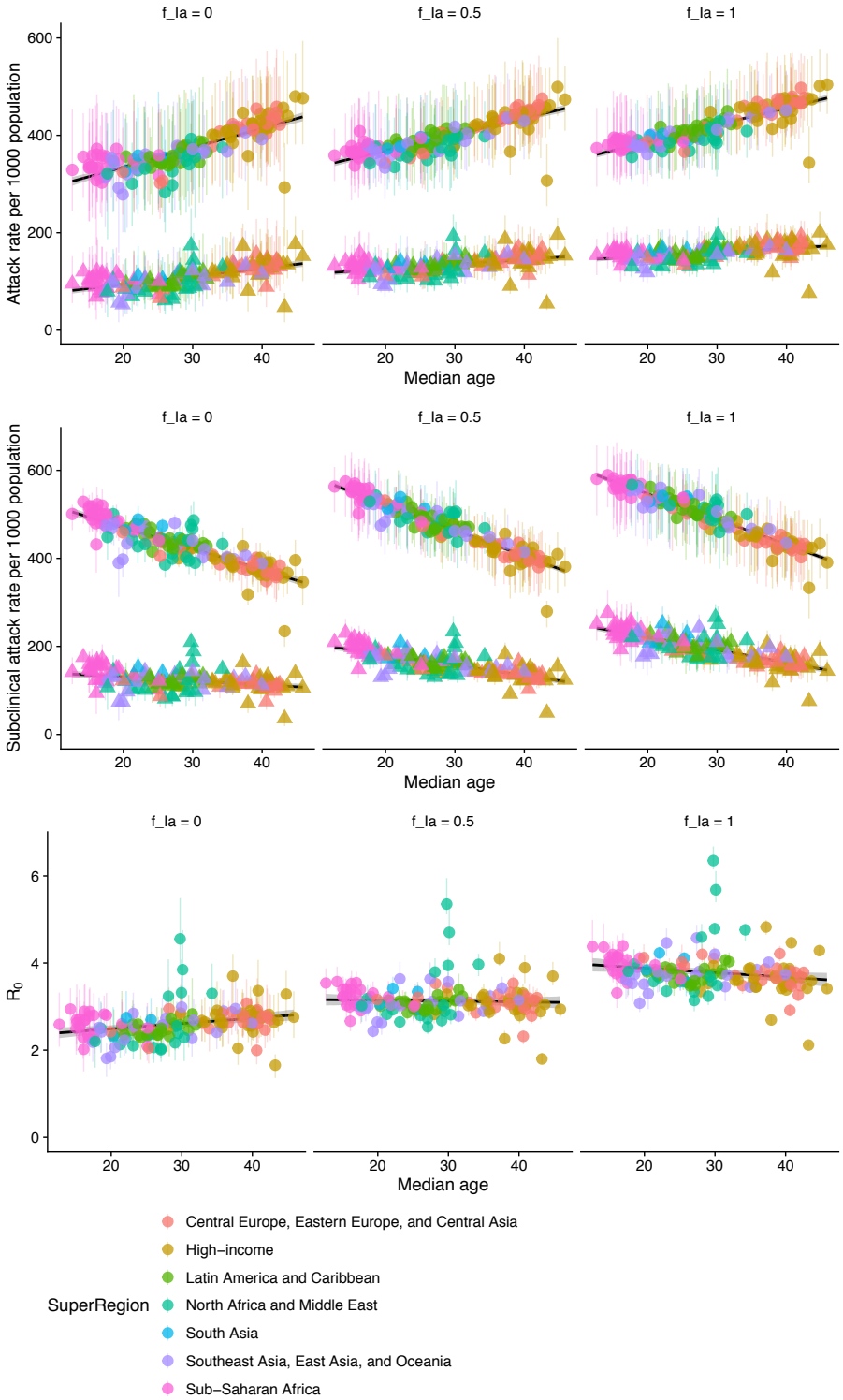

Extended Data Figure 6. (a) Projected total and peak clinical case attack rate for 146 capital cities, under different assumptions for the infectiousness of subclinical infections. **(b)** Projected total and peak subclinical infection attack rate for 146 capital cities, under different assumptions for the infectiousness of subclinical infections. **(c)** Projected differences in R0 among 146 capital cities, under different assumptions for the infectiousness of subclinical infections.

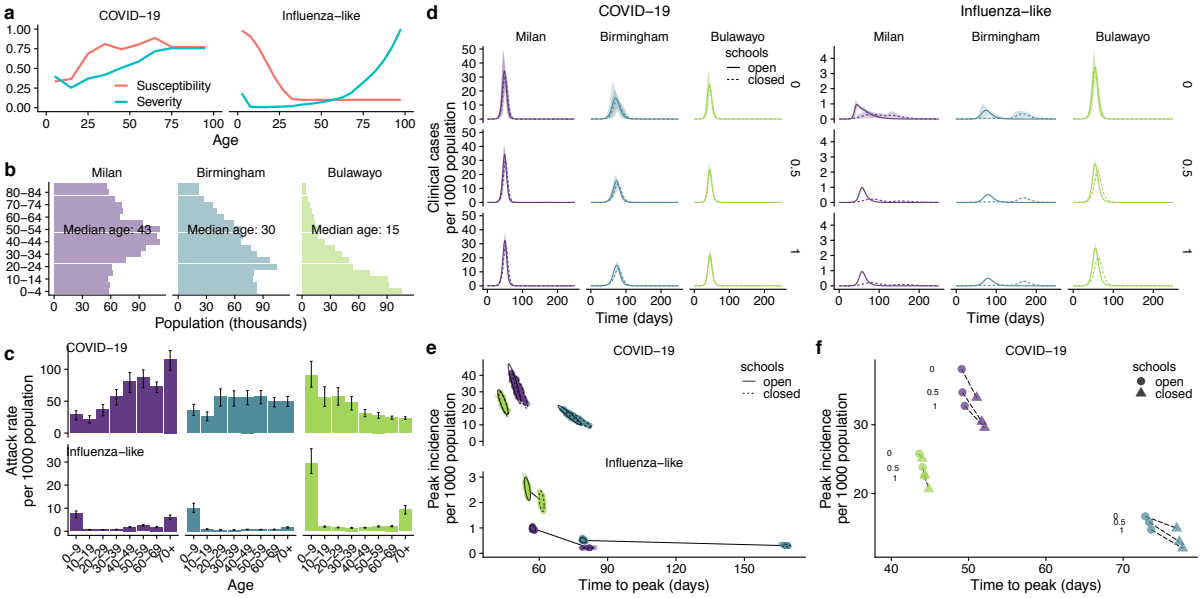

Extended Data Figure 7. Comparison of school closures in three exemplar cities when susceptibility u_i is fixed across settings instead of R0.

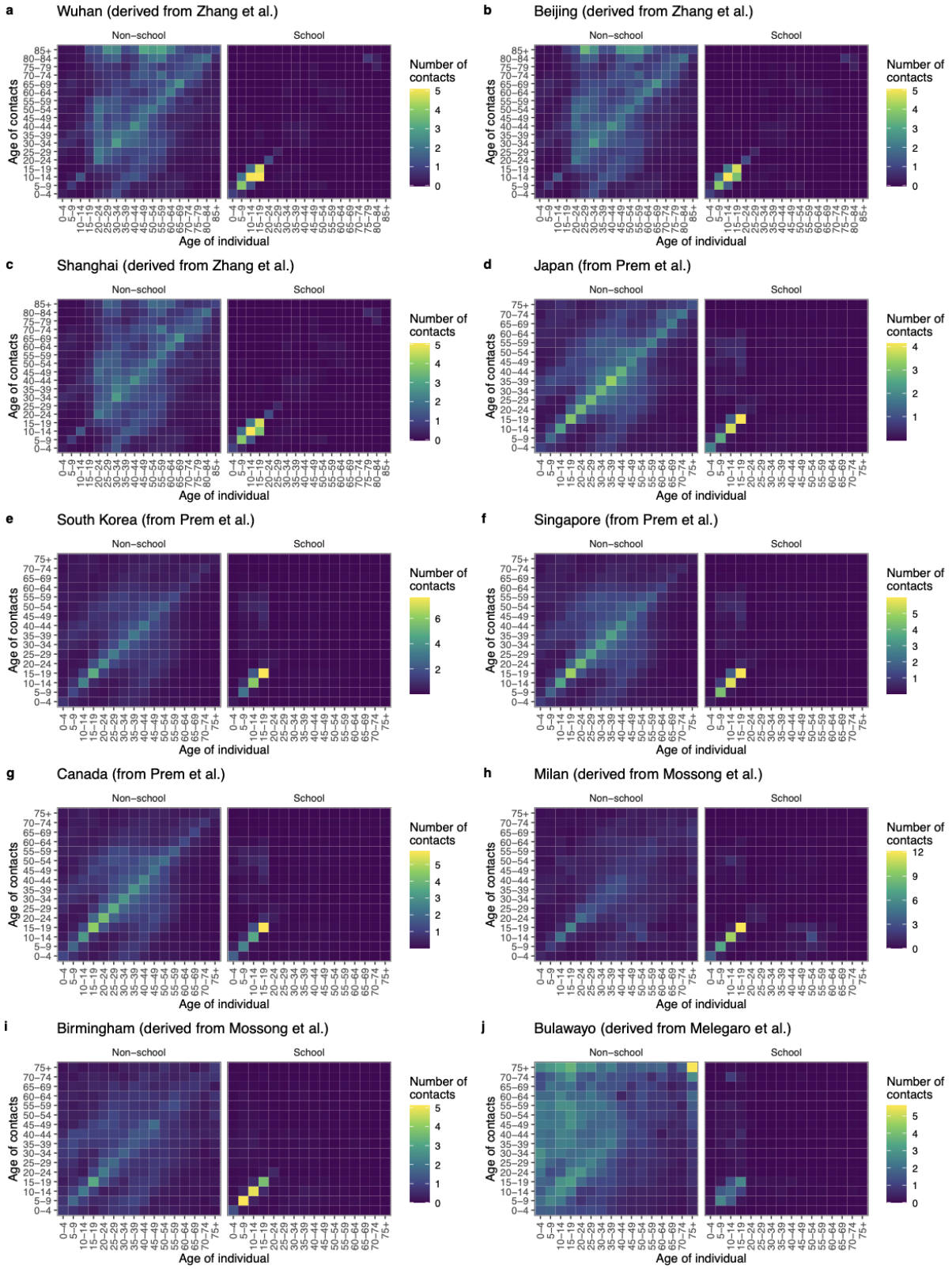

Extended Data Figure 8. Contact matrices used for Figs. 1-3 of the main text. We have not shown matrices for all 12 regions of Italy modelled, nor for all 13 provinces of China modelled, as these show similar patterns to the matrices for Milan and for Wuhan, Beijing and Shanghai, respectively.

Supplementary Information

Age-dependent effects in the transmission and control of COVID-19 epidemics

Authors: Nicholas G. Davies[1*], Petra Klepac[1^], Yang Liu[1^], Kiesha Prem[1], Mark Jit[1], CMMID COVID-19 working group, Rosalind M Eggo[1*]

The CMMID COVID-19 working group[1] is: Carl A B Pearson, Billy J Quilty, Adam J Kucharski, Hamish Gibbs, Samuel Clifford, Amy Gimma, Kevin van Zandvoort, James D Munday, Charlie Diamond, W John Edmunds, Rein MGJ Houben, Joel Hellewell, Timothy W Russell, Sam Abbott, Sebastian Funk, Nikos I Bosse, Fiona Sun, Stefan Flasche, Alicia Rosello & Christopher I Jarvis. Order of working group determined at random.

[1] Department of Infectious Disease Epidemiology, London School of Hygiene & Tropical Medicine, Keppel Street, WC1E 7HT
^ these authors contributed equally
* correspondence to Rosalind M Eggo r.eggo@lshtm.ac.uk or Nicholas G Davies nicholas.davies@lshtm.ac.uk

Parameter	Description	Prior
u_i	Susceptibility to infection upon contact with an infectious person	Non-age-varying: $u_i \sim normal(\mu = 0.1, \sigma = 0.025, min = 0)$ Age-varying: young, middle, and old age fit as $a_y \sim normal(\mu = 15, \sigma = 15, min = 0, max = 30)$ $a_m \sim normal(\mu = 45, \sigma = 15, min = 30, max = 60)$ $a_o \sim normal(\mu = 75, \sigma = 15, min = 60, max = 90)$ Susceptibility for young, middle, and old age fit as $u_y \sim normal(\mu = 0.1, \sigma = 0.025, min = 0)$ $u_m \sim normal(\mu = 0.1, \sigma = 0.025, min = 0)$ $u_o \sim normal(\mu = 0.1, \sigma = 0.025, min = 0)$ Then $u_i = coss(i \mid a_y, b_y, a_m, b_m, a_o, b_o)$ (see final row)
y_i	Clinical fraction on infection	Non-age-varying: $y_i = 0.5$ Age-varying: young, middle, and old age fit as $a_y \sim normal(\mu = 15, \sigma = 15, min = 0, max = 30)$ $a_m \sim normal(\mu = 45, \sigma = 15, min = 30, max = 60)$ $a_o \sim normal(\mu = 75, \sigma = 15, min = 60, max = 90)$ Susceptibility for young, middle, and old age fit as $y_y \sim normal(\mu = 0.5, \sigma = 0.1, min = 0, max = 0.5)$ $y_m = 0.5$ $y_o \sim normal(\mu = 0.5, \sigma = 0.1, min = 0.5, max = 1)$ Then $y_i = coss(i \mid a_y, y_y, a_m, y_m, a_o, y_o)$ (see below)
t_{seed}	Timing of introduction of cases	$t_{seed} \sim normal(\mu = 15, \sigma = 30, min = 0, max = 30)$
q_H	Multiplicative factor for transmission during holiday period	$q_H \sim beta(\alpha = 2, \beta = 2)\ scaled\ to\ 0 - 2$
q_L	Multiplicative factor for transmission during large-scale restrictions	$q_L \sim beta(\alpha = 2, \beta = 2)$
A_{min}, A_{max}	Age bounds for introduced cases	$A \sim normal(\mu = 60, \sigma = 20, min = 40, max = 80)$ $A_{range} \sim beta(\alpha = 2, \beta = 2)\ scaled\ to\ 0 - 10$ $A_{min} = A - A_{range}$ $A_{max} = A + A_{range}$
$coss(a \mid x_1, y_1, x_2, y_2, x_3, y_3)$	Cosine-smoothing function	For a given age *a* (the midpoint age of age group *i*) the function evaluates to y_1 for $a \leq x_1$, to y_2 for $a = x_2$, and to y_3 for $a \geq x_3$. Values of a between x_1 and x_2 are interpolated between y_1 and y_2, and values of a between x_2 and x_3 are interpolated between y_2 and y_3, where the interpolation takes the shape of a cosine curve between $-\pi$ and π.

Supplementary Table 1. Details of model fitting.

Location	**Mixing matrix details**
Wuhan City, China	We used mixing matrices measured in Shanghai in 2017/2018[6], adapted to the demographics of Wuhan prefecture. This implicitly assumes that Shanghai mixing patterns are representative of large cities in China.
Regions of China: Anhui, Guangdong, Guangxi, Hubei, Hunan, Jiangsu, Jiangxi, Jilin Shaanxi, Shandong, Sichuan, Tianjin, Zheijiang provinces; Beijing, Shanghai.	We used mixing matrices measured in Shanghai in 2017/2018[6], adapted to the demographics of each province / city.
Regions of Italy: Lombardia, Piemonte, Trento Veneto, Friulli Venezia Giulia, Liguria, Emilia-Romagna, Toscana, Marche, Lazio, Campania, Puglia regions; Milan.	We used mixing matrices measured in Italy in 2005/2006[7], adapted to the demographics of each region / city. This assumes that these contact patterns will still be representative of contact patterns in 2020.
Ontario, Canada	We used synthetic contact matrices, generated based on demographic information about the country[8].
Japan	We used synthetic contact matrices, generated based on demographic information about the country[8].
Singapore	We used synthetic contact matrices based on demographic information about the country[8].
South Korea	We used synthetic contact matrices based on demographic information about the country[8].
Birmingham, UK	We used mixing matrices measured in the UK in 2005/2006[7], adapted to the demographics of Birmingham. This assumes that these contact patterns will still be representative of contact patterns in 2020.
Bulawayo, Zimbabwe	We used mixing matrices measured in Manicaland, Zimbabwe in 2013[9], adapted to the demographics of Bulawayo. This implicitly assumes that Manicaland mixing patterns are representative of Bulawayo.
150 capital cities	We used synthetic contact matrices, generated based on demographic information about each country[8].

Supplementary Table 2. Details on mixing matrices used in the study.

Wuhan: Model 1		
age_y	6	(4.2-7.2)
age_m	55	(46-60)
age_o	64	(60-68)
susc_y	0.003	(0.00014-0.0076)
susc_m	0.044	(0.032-0.054)
susc_o	0.084	(0.079-0.09)
seed_start	19	(16-22)
seed_age	61	(42-79)
seed_age_range	4.9	(1.5-8.9)
qH	1.4	(1.3-1.5)
qL	0.41	(0.3-0.56)
Wuhan: Model 2		
age_y	19	(14-29)
age_m	50	(40-60)
age_o	68	(60-79)
susc	0.055	(0.052-0.059)
symp_y	0.037	(0.0051-0.062)
symp_m	0.3	(0.19-0.42)
symp_o	0.65	(0.52-0.77)
seed_start	16	(14-20)
seed_age	46	(30-67)
seed_age_range	1.3	(0.5-1.9)
qH	1.3	(1.2-1.4)
qL	0.43	(0.31-0.56)
Wuhan: Model 3		
susc	0.046	(0.045-0.048)
seed_start	20	(17-21)
seed_age	64	(37-80)
seed_age_range	4.2	(0.93-8.7)
qH	1.4	(1.3-1.5)
qL	0.33	(0.21-0.42)
Beijing, Shanghai		
susc	0.062	(0.05-0.077)
B_seed_t0	18	(8.7-23)
S_seed_t0	19	(12-25)
seed_d	3.1	(0.74-6.3)
lockdown_t	54	(53-56)
qH	1.3	(0.89-1.8)
qL	0.19	(0.15-0.25)
South Korea		
susc	0.098	(0.087-0.11)
seed_t0	9.2	(4.9-13)
seed_d	3.3	(0.73-6)
lockdown_t	53	(52-54)
qL	0.052	(0.0011-0.1)
Lombardy		
susc	0.084	(0.075-0.096)
conf_mean	7.6	(2.7-13)
conf_shape	11	(3.7-20)
onset_known	0.36	(0.061-0.62)
seed_t0	15	(11-20)
seed_d	3.6	(0.83-6.3)
lockdown_t	50	(47-54)
qL	0.48	(0.28-0.72)

Supplementary Table 3. Posterior means and 95% HDIs from fitting the dynamic transmission model (Figs. 1 and 2, main text).